Metallomics

PAPER

Metal sensing and signal transduction by CnrX from *Cupriavidus metallidurans* CH34: role of the only methionine assessed by a functional, spectroscopic, and theoretical study†

Cite this: *Metallomics*, 2014, 6, 263

Juliette Trepreau,[a] Cornelia Grosse,[b] Jean-Marie Mouesca,[c] Géraldine Sarret,[d] Eric Girard,[a] Isabelle Petit-Haertlein,[a] Sandra Kuennemann,[b] Céline Desbourdes,[a] Eve de Rosny,[a] Antoine P. Maillard,[a] Dietrich H. Nies[b] and Jacques Covès*[a]

Received 10th September 2013,
Accepted 2nd October 2013

DOI: 10.1039/c3mt00248a

www.rsc.org/metallomics

When CnrX, the periplasmic sensor protein in the CnrYXH transmembrane signal transduction complex of *Cupriavidus metallidurans* CH34, binds the cognate metal ions Ni(II) or Co(II), the ECF-type sigma factor CnrH is made available in the cytoplasm for the RNA-polymerase to initiate transcription at the *cnrYp* and *cnrCp* promoters. Ni(II) or Co(II) are sensed by a metal-binding site with a N_3O_2S coordination sphere with octahedral geometry, where S stands for the thioether sulfur of the only methionine (Met123) residue of CnrX. The M123A-CnrX derivative has dramatically reduced signal propagation in response to metal sensing while the X-ray structure of Ni-bound M123A-CnrXs showed that the metal-binding site was not affected by the mutation. Ni(II) remained six-coordinate in M123A-CnrXs, with a water molecule replacing the sulfur as the sixth ligand. H32A-CnrXs, the soluble model of the wild-type membrane-anchored CnrX, was compared to the double mutants H32A-M123A-CnrXs and H32A-M123C-CnrXs to spectroscopically evaluate the role of this unique ligand in the binding site of Ni or Co. The Co- and Ni-bound forms of the protein display unusually blue-shifted visible spectra. TD-DFT calculations using structure-based models allowed identification and assignment of the electronic transitions of Co-bound form of the protein and its M123A derivative. Among them, the signature of the S–Co transition is distinguishable in the shoulder at 530 nm. *In vitro* affinity measurements point out the crucial role of Met123 in the selectivity for Ni or Co, and *in vivo* data support the conclusion that Met123 is a trigger of the signal transduction.

Introduction

The aerobic β-proteobacterium *Cupriavidus metallidurans* CH34 of the order *Burkholderiales* prevails in heavy-metal rich environments. Its collection of genetic determinants for metal resistance makes it the archetype of heavy-metal resistant bacteria.[1–4] Redundant RND‡ (resistance nodulation and cell division) heavy metal efflux pumps are the major actors of this resistance. RND-driven transenvelope protein complexes adjust the periplasmic cation composition by pumping surplus cations, which have entered this compartment, back to the outside.[5] The most prominent RND complexes are CzcCBA (cobalt, zinc and cadmium), CnrCBA (cobalt and nickel), CusCBA and SilCBA (both for copper and silver).[3,5] During surplus levels of Ni(II) in the cytoplasm, these systems are assisted by inner membrane exporters such as CnrT and DmeF.[6] Periplasmic metal cation

[a] *Institut de Biologie Structurale, UMR 5075 CNRS-CEA-UJF-Grenoble-1, 6 Rue Jules Horowitz, 38042 Grenoble, France. E-mail: jacques.coves@ibs.fr; Tel: +33-(0)4-57-42-85-16*
[b] *Institute for Biology/Microbiology, Martin-Luther-University, Kurt-Mothes-Str. 3, 06099 Halle/Saale, Germany*
[c] *Laboratoire de Résonance Magnétique, Service de Chimie Inorganique et Biologique, UMR E3 CEA-UJF, Institut des Nanotechnologies et Cryogénie, CEA-Grenoble, 38054 Grenoble Cedex 9, France*
[d] *ISTerre, Institut des Sciences de la Terre, Université Grenoble I, CNRS, 38041 Grenoble, France*

† Electronic supplementary information (ESI) available. See DOI: 10.1039/c3mt00248a

‡ The abbreviations used are: ECF, extracytoplasmic function; EGTA, ethyleneglycoltetraacetic acid; EXAFS, extended X-ray absorption fine structure; LFT, ligand field transition; LMCT, ligand-to-metal charge transfer; MIC, minimum inhibitory concentration; RMSD, root-mean-square deviation; RND, resistance nodulation and cell division; TD-DFT, time-dependent density functional theory; TMM, Tris-buffered mineral salts medium; XANES, X-ray absorption near edge spectroscopy; XAS, X-ray absorption spectroscopy.

concentrations also serve as signals to regulate expression of the operons encoding these efflux pumps. Two-component signal transduction systems are predominantly used to couple signal sensing and regulation in bacteria.[7] However, alternative sigma factors of the extracytoplasmic function family (ECF) can also relay the response of extracytoplasmic stimuli to the cytoplasm.[8,9]

For instance, the CnrCBA efflux pump is encoded by the *cnr* determinant which is controlled by the three-protein transmembrane signal transduction complex CnrYXH.[10–13] CnrH is an ECF-type sigma factor required for transcription initiation at *cnr* promoters. Thought to be sequestered at the membrane by the anti-sigma protein CnrY, CnrH can be made available to activate RNA-polymerase upon sensing of increasing amount of Ni or Co in the environment by CnrX. The presence of both proteins, CnrY and CnrX, seems to be essential for sequestration of CnrH in the absence of nickel or cobalt.[13] To better understand CnrYXH transmembrane signal transduction, we recently established the structural basis of metal sensing by CnrX.[14] CnrX is a membrane-anchored dimeric protein with a C-terminal periplasmic metal-sensor domain (CnrXs) that spans residues 31 to 148. The three-dimensional structure of CnrXs determined with Ni, Co or Zn bound to the protein revealed one metal-binding site per monomer. It is likely that Zn-bound CnrXs represents an inactive form of the complex, while replacement of Zn with either Ni or Co ions elicits a biological response.[14,15] This substitution results in a dramatic change in the geometry of the metal-binding site in addition to remodeling of the four-helix bundle harboring it. While the Zn ion is pentacoordinated in a N_3O_2 sphere (the Nε2 atoms of His42, His46, and His119, and two O atoms of Glu63), Ni or Co ions recruit the thioether sulfur of the only CnrXs methionine (Met123) as the sixth ligand. The geometry therefore moves from trigonal bipyramidal in the presence of Zn to octahedral in the presence of Ni or Co with the consequence to tune the whole packing of the CnrX dimer.[14] It is noteworthy that these residues are strictly conserved in the CnrX family of proteins.[14] We hypothesized that the recruitment of the Met123 side chain initiates the sensing mechanism. His42, His46 and His119 have already been described as important for nickel-dependent induction of *cnr*.[13] The bonding of metal ions in metalloproteins *via* the side chain of a methionine is quite rare and, to our knowledge, has never been observed for Co(II), except when this metal ion was used in the substitution of Cu(II) as in azurin or rusticyanin.[16,17] This prompted us to spectroscopically characterize this novel type of coordination sphere [UV-visible spectroscopy and X-ray absorption spectroscopy (XAS)] and to probe the biological function of Met123 in CnrX by studying *in vivo* the behavior of a *C. metallidurans* strain harboring a M123A-CnrX derivative. In addition, theoretical calculations using time-dependent density functional theory (TD-DFT) evaluated the contribution of the thioether sulfur from Met123 to the unusually blue-shifted UV-visible spectra. Our main conclusions are that Met123 plays a crucial role in both metal selectivity and affinity, and is a key player in the signal transduction of the CnrYXH complex.

Experimental

Bacterial strains and growth conditions

C. metallidurans DN190(pMOL28-3 Δ*cnrYXH* Φ*cnrCBA-lacZ*),[11] the test strain used in this study, is a mutant strain of AE126(pMOL28). Strain AE126 is a derivative of CH34(pMOL28, pMOL30) wild type that contains only the *cnr* plasmid pMOL28.[1] In the test strain plasmid pMOL30 is missing, a *lacZ* transcriptional fusion was inserted downstream of the *cnrCBA* operon, and the regulatory genes *cnrYXH* were deleted. This strain was complemented *in trans* with the derivatives of plasmid pBBR1-MCS2.[18] The plasmid contained no insert (negative vector control), an unchanged *cnrYXH* operon (positive control) or a *cnrYXH* operon with a mutated *cnrX* gene. Each operon was cloned either in the direction of the *lacZp* promoter on plasmid pBBR1 or against it. Thus, in the resulting pBBR1-containing DN190 strain, the *lacZp* promoter is on vector pBBR1 but the *lacZ* gene is on plasmid pMOL28-3 as part of the *cnrCBA* operon under the control of the CnrH-dependent *cnrCp* promoter (Fig. SI1, ESI†). The *lacZp* promoter is constitutive in *C. metallidurans* because this bacterium does not contain a *lac* operon.[19] The *cnrYXH* operon contained its own promoter *cnrYp*[11] that also depends on CnrH; however, the mutant CnrX derivative might lead to a situation where the release of CnrH from CnrYX is prevented. This might result in a negative cooperative cycle that completely abolishes any expression of *cnrYXH*. To prevent this possibility, the *cnrYXH* mutant and parent operons were cloned in plasmid pBBR1 in both orientations with respect to the *lacZp* promoter residing on the vector (Fig. SI1, ESI†). The release of CnrH from the CnrYXH protein complex is necessary to initiate transcription from *cnrCp* and thus expression of Φ(*cnrCBA-lacZ*). Tris-buffered mineral salts medium[1] containing 2 g of sodium gluconate per l (TMM) was used to aerobically cultivate these strains with shaking at 30 °C. Analytical grade salts of heavy metal chlorides were used to prepare 1 M stock solutions, which were sterilized by filtration. Solid Tris-buffered media contained 20 g agar per l.

For the minimum inhibitory concentration (MIC) determination, the cells were cultivated in TMM for 30 h at 30 °C with shaking, diluted 20-fold into fresh TMM, cultivated for another 24 h, diluted 100-fold into fresh TMM, streaked onto TMM plates containing increasing concentrations of nickel or cobalt chloride and incubated for 5 days at 30 °C.

Genetic techniques

Standard molecular genetic techniques were used.[20,21] For conjugative gene transfer, overnight cultures of donor strain *E. coli* S17/1[22] and of the *C. metallidurans* recipient strains grown at 30 °C in Tris-buffered medium were mixed (1 : 1) and plated onto nutrient broth agar. After 2 days, the bacteria were suspended in TMM, diluted, and plated onto selective media as previously described.[20]

Induction experiments

C. metallidurans cells with a *lacZ*-reporter gene fusion were cultivated in TMM with shaking at 30 °C. At a cell density of 60–70 Klett units, 0.5 mM $NiCl_2$ was added and cells were

incubated with shaking for an additional 3 h. A control experiment without the addition of metal ion was run in parallel. Samples were taken every 30 min and the specific β-galactosidase activity was measured in permeabilized cells as published previously with 1 U defined as the activity forming 1 nmol of *o*-nitrophenol per min at 30 °C.[23]

Site-directed mutagenesis and protein preparation

The overexpression plasmid pET-H32A-CnrXs[14] was used as a matrix to produce the H32A-M123A double-mutation in CnrXs. The forward and reverse sequences for the M123A mutation were GACCTTGGTTCACGTGTTTGAAGCGCGTGCGGGCC and GGCCCGCACGCGCTTCAAACACGTGAACCAAGGTC, respectively. Those for the M123C mutation were GACCTTGGTTCACGTGTTT GAATGCCGTGCGGGCC and GGCCCGCACGGCATTCAAACACGT GAACCAAGGTC, respectively. The mismatch positions corresponding to the replacement of the ATG codon (Met) by GCG (Ala) or TGC (Cys) are underlined. The QuikChange™ Site-Directed Mutagenesis kit from Stratagene was used as specified by the manufacturer. Mutations were confirmed by DNA sequencing and the new construct was transformed into *E. coli* BL21(DE3). H32A-M123A-CnrXs was overproduced and purified as previously described for H32A-CnrXs.[14] Protein concentrations were determined using the Bradford[24] protein assay (BioRad) with bovine serum albumin as standard. Throughout this article, CnrXs (wild-type or mutants) refers to a dimer. Consequently, all the concentrations given are those of the dimeric protein and the molar ratios are calculated for a dimer.

Biochemical methods

For the determination of the affinity of the CnrXs mutants for Co and Zn, mag-fura-2 was used in competition experiments, except for H32A-CnrXs and Co for which the competitor was fura-2. The dyes (Invitrogen, Molecular Probes) were dissolved in ultra pure water (CHROMASOLV®, Sigma-Aldrich) and added at a final concentration of about 7 μM into a protein solution at 25 μM in 50 mM Hepes pH 7.5 treated with Chelex (BioRad). The exact concentration of the dye or the protein was determined in each experiment using their extinction coefficients at 362 nm or 280 nm, respectively. The mixture was titrated by iterative addition of freshly prepared $CoCl_2$ or $ZnCl_2$ so that the final volume changes were less than 4%. Mag-fura-2 and fura-2 isotherms were fit to a single site model using the program Dynafit.[25] For mag-fura-2/Co, we used the dissociation constant of 9.3×10^{-7} M reported in the literature.[26] For fura-2/Co and mag-fura-2/Zn, we determined experimentally the dissociation constants by competition assay with EGTA, using the single site model and K_d at pH 7.5 of 8.1×10^{-10} M and of 4.0×10^{-8} M for EGTA/Co and EGTA/Zn, respectively.[27] The resulting K_d were 2.4×10^{-10} M for fura-2/Co and 4.0×10^{-8} M for mag-fura-2/Zn.

For Western blot analysis, cells were cultivated in TMM for 30 h at 30 °C with shaking, diluted 200-fold into fresh TMM, divided into two sub-cultures, and cultivated for another 24 h in the presence of either 0.5 mM $NiCl_2$ or no added metal. Cells were harvested by centrifugation (2 min, 16 000×*g*, 4 °C) and suspended in buffer (100 mM Tris-HCl, pH 8.0). Crude extracts from 35 μg dry mass of cells were separated by 15% (w/v) SDS-PAGE, blotted onto a PVDF membrane, and visualized using a polyclonal anti-CnrXs antibody.

Spectroscopic methods. UV-visible and X-ray absorption spectroscopy (XAS) measurements were performed as already described.[15] The technical conditions for XAS are given in brief hereafter. XAS measurements were carried out at the European Synchrotron Radiation Facility (ESRF, Grenoble, France) which was operating with a ring current of 150 to 200 mA. Spectra were collected on the BM30B (FAME) beamline using a Si(220) double crystal monochromator with dynamic sagittal focusing. Details of the experimental setup and the data treatment procedure, including fit of multiple scattering contributions arising from imidazole rings, are given in ESI.† When required, specific experimental conditions are given in the figure captions.

Crystallization, structure determination and refinement

Crystals were obtained by mixing 2 μL of M123A-CnrXs protein, loaded with either 4 Co(II) equiv. or 4 Ni(II) equiv., with 2 μL of solution consisting of 16–20% PEG 2000 MME and 15% glycerol, as previously described for E63Q-CnrXs.[14] Before data collection, crystals were harvested in a loop, soaked in the mother liquor adjusted to 20% glycerol for a few seconds and then transferred into paraffin oil prior to cryocooling in liquid nitrogen. Diffraction data were collected at ESRF beamline ID23-2 (ESRF-Grenoble). Diffraction data were integrated with XDS[28] and integrated intensities were scaled and merged using AIMLESS and TRUNCATE from the CCP4 suite of programs.[29] The percentage of correlation between intensities from random half-datasets (CC1/2) was calculated as described.[30] Crystals belonged to the $P2_1$ space group leading to two dimers in the asymmetric unit. Data analysis with the XTRIAGE module in PHENIX[31] indicated the presence of twinning (fraction of 0.40). The structure of Ni-bound M123A-CnrXs at 1.85 Å resolution was determined by molecular replacement using the program PHASER.[32] In order to limit bias in the metal binding site that may arise from the search model, the structure of the *apo*-form of CnrXs represented by E63Q-CnrXs (PDB entry: 2y3h)[14] was used through a polyAla model. Hendrickson-Lattman coefficient, as provided by PHASER, was improved using DM[33] prior to automatic model building with Buccanneer.[34] The resulting model was manually completed in COOT.[35] Refinement was carried out with PHENIX using the standard detwinning procedure implemented within the program. The model was then optimized through iterative rounds of refinement and manual model building. Diffraction data and refinement statistics are summarized in Table SI1 (ESI†). Coordinates and structure factors have been deposited in the Protein Data Bank with accession number 3zg1.

Molecular models and TD-DFT methodology

To identify the specific features of the UV-visible absorption spectra recorded for Co-bound H32A-CnrXs and H32A-M123A-CnrXs, we designed two molecular models of the corresponding metal-binding sites. In the following, 'Imd' stands for an

imidazole group modeling the histidine residues 42, 46 and 119. The methionine residue 123 and the glutamate residue 63 have been replaced by the $S(CH_3)_2$ group and CH_3CO_2 moieties, respectively. These ligand models were given the minimal molecular size required to reach reliable electronic transition energies. This was checked by testing the series SH_2, $S(CH_3)_2$ and $S(CH_2CH_3)_2$. The first molecular model $[CoS(CH_3)_2(Imd)_3(CH_3CO_2)]^{1+}$ (S = 3/2) called "Co-Met", and designed to mimic the cobalt-binding site of Co-bound H32A-CnrXs, was directly constructed from crystallographic data. All heavy atoms have been placed at their respective crystallographic positions (PDB entry 2y3b; resolution 1.55 Å).[14] Notice, in particular, that the distance Co–S is 2.54 Å. For Co-bound H32A-M123A-CnrXs, a second molecular model $[Co(H_2O)(Imd)_3(CH_3CO_2)]^{1+}$ (S = 3/2) called "Co-Wat" was built from Co-Met by replacing $S(CH_3)_2$ with a water molecule. The Co–O distance was set at 2.2 Å, identical to the Ni–O_{Wat} crystallographic distance measured in the corresponding Ni-bound M123A-CnrXs: PDB entry 3zg1 (this work, see below) without further geometry-optimization.

In order to perform the TD-DFT calculations, we used the Slater-based ADF2009 code[36] with triple-ζ (all-electron) basis sets for all atoms. We relied on the SAOP (Statistical Average Of Potential) exchange-potential,[37] specifically designed to exhibit the proper $(-1/r)$ asymptotic behavior outside the molecular model. The simulated spectra have been generated by taking into account all first 30 excitations $\{E_i\}_{i=1-30}$ yielded by the implemented TD-DFT procedure (Davidson's algorithm).[38,39] Notice that no *a priori* selection of the transitions has been performed. The analytical expression used for the simulated spectra is as follows: $\Sigma_{i=1-30} f_i \times [10^6/\sigma\cdot\mathrm{sqrt}(\pi)]\cdot\exp - [(8066 \times 1240/\sigma^2)\cdot(1/E - 1/E_i)]$, where f_i is the oscillator strength for transition i, σ defines a common broadness factor for the peaks of a given spectrum, determined visually in each case (see the legend of Fig. 7), E and E_i are expressed in wavelength units (nm), and 8066 and 1240 are appropriate conversion factors (1240/nm = eV and eV × 8066 = cm^{-1}).

Results

Biological function of M123A-CnrX

To characterize the influence of the only methionine of CnrX on the biological function of this protein, the M123A mutation was introduced into the *cnrYXH* gene region by site-directed mutagenesis. The mutated *cnrYXH* operon was cloned into plasmid pBBR1 and transferred into *C. metallidurans* strain DN190(pMOL28-3, Φ(*cnrCBA-lacZ*) Δ*cnrYXH*). As described in the experimental section and illustrated in Fig. SI1 (ESI†), in the "Yp − Zp" situation, *cnrYXH* should be solely expressed from *cnrYp*. In contrast, in the "Yp + Zp" situation, *cnrYXH* was cloned under the control of the *lacZp* promoter, which is constitutive in *C. metallidurans* and should mediate constitutive expression of *cnrYXH* in addition to any transcription initiation starting from *cnrYp*.

As published, strain AE126 with the native plasmid pMOL28 produced CnrX only when the cells were challenged with 0.5 mM Ni(II) (Fig. 1, panel A, AE126).[13] Due to the deletion of the *cnrYXH* region in plasmid pMOL28-3, cells of strain DN190 failed to synthesize CnrX when they only carried the vector plasmid pBBR1 (Fig. 1, panel A, vector). When they contained a pBBR1 vector with the *cnrYXH* wild-type region, a strong CnrX signal appeared in Ni(II)-challenged cells. Without Ni(II), a faint CnrX band was visible only when the *cnrYXH* region was cloned in the "Yp + Zp" orientation (Fig. 1, panel A, wild-type). When the pBBR1 plasmid harbored a mutated *cnrYXH* operon that synthesizes the M123A-CnrX derivative, a CnrX signal appeared only when the respective operon was cloned in the "Yp + Zp" orientation (Fig. 1, panel B). The intensity of this signal did not differ whether the cells were cultivated in the presence of nickel ions or not. This demonstrated that (i) M123A-CnrX was stable in *C. metallidurans* strain DN190; (ii) synthesis of the CnrYXH protein complex with the M123A-CnrX did not yield sufficient CnrH for effective expression of the *cnrYXH* operon; (iii) presence of Ni(II) no longer increased the availability of CnrH.

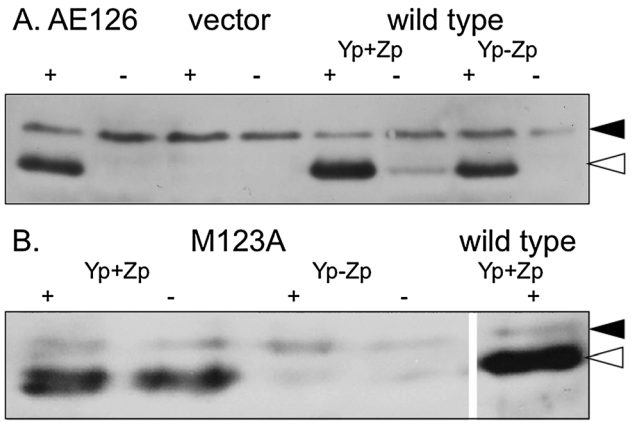

Fig. 1 Production of CnrX mutant derivatives. Western blots show the production of CnrX in the cells of *C. metallidurans* strains AE126(pMOL28) or DN190(pMOL28-3(Δ*cnrYXH* Φ*cnrCBA-lacZ*), pBBR1). Cells were incubated in the presence (+) or absence (–) of 0.5 mM Ni(II) and harvested. The crude extract was separated by polyacrylamide gel electrophoresis, the gels were blotted, and CnrX was visualized using polyclonal anti-CnrX antibodies. Contrast and brightness changed with Photoshop. Panel A is a control experiment. It shows the production of CnrX wild type from the native plasmid pMOL28 in strain AE126 (left two lanes), from pMOL28-3(Δ*cnrYXH* Φ*cnrCBA-lacZ*) in strain DN190 additionally containing only the vector pBBR1, or containing plasmid pBBR1 with the *cnrYXH* wild type region cloned in the "Yp + Zp" or "Yp − Zp" orientation. Panel B shows expression of only the M123A-CnrX derivative when the mutant *cnrYXH* region was cloned in the "Yp + Zp" orientation but merely a faint signal in "Yp − Zp". The control in panel B was the wild type region in "Yp + Zp" on the same blot but in a distant lane. Open arrowhead: CnrX-specific signal; closed arrowhead: unspecific signal that is also visible in the DN190/pBBR1 vector control.

The reporter gene activity of the Φ(*cnrCBA-lacZ*) fusion on plasmid pMOL28-3 in strain DN190 with the pBBR1-derivatives was also determined. When the cells containing the *cnrYXH* wild type region *in trans* to pMOL28-3 were stimulated with 0.5 mM Ni(II), the specific β-galactosidase activity increased with rates of 148 U mg^{-1} h^{-1} and 70 U mg^{-1} h^{-1} when the operon was in the Yp − Zp and Yp + Zp orientations, respectively (Fig. 2). The activity did not increase when the cells were

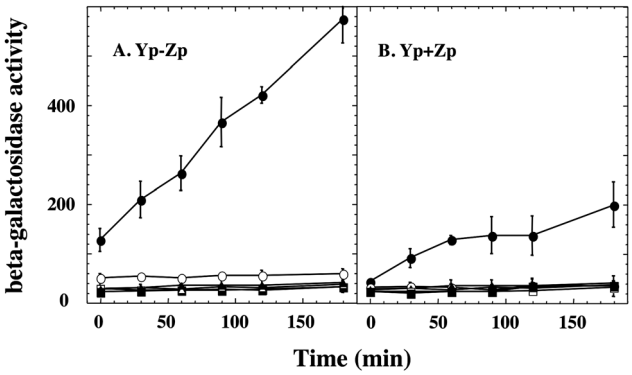

Fig. 2 Expression of Φ*cnrCBA-lacZ*. M123A-CnrX was not able to stimulate expression of Φ*cnrCBA-lacZ in trans*. *C. metallidurans* strain DN190(pMOL28-3 Δ*cnrYXH* Φ*cnrCBA-lacZ*), additionally containing a pBBR1 derivative with the *cnrYXH* region in the "Yp − Zp" (panel A) or "Yp + Zp" (panel B) orientation, was cultivated in TMM for 30 h at 30 °C, diluted to 30 Klett units with fresh TMM, and incubated with shaking until the turbidity reached 60 Klett units. This culture was divided into sub-cultures that were incubated with shaking at 30 °C in the presence of 0.5 mM Ni(II) (closed symbols) or no metal (open symbols). Samples were removed every 0.5 h until 3 h was reached, and the specific β-galactosidase activity in U mg^{-1} dry mass was determined. Each experiment was performed three or four times; deviation bars are shown. The pBBR1-plasmids contained wild-type *cnrYXH* (circles), the M123A-CnrX mutant region (squares) or no insert (triangles, shown in both panels).

incubated in the absence of Ni(II). When the DN190 cells instead contained the mutated *cnrYXH* region, which encodes the M123A-CnrX region, neither the absence nor presence of Ni(II) resulted in increased activity. Therefore, the mutated *cnrYXH* region did not provide sufficient CnrH to initiate transcription of the Φ(*cnrCBA-lacZ*) fusion from the *cnrYp* promoter.

The MIC values for Ni(II) and Co(II) were in agreement with this result. Three independent experiments were performed with identical outcomes. The MIC values for DN190 with the pBBR1 vector control were 1.0 mM Ni(II) and 0.5 mM Co(II). With pBBR1 containing the *cnrYXH* wild type region in either orientation, they were 5 mM Ni(II) and 4 mM Co(II), and for pBBR1 containing the mutated *cnrYXH* region they were 2 mM Ni(II) and 1 mM Co(II) (Yp − Zp) or 1.5 mM Ni(II) and 1 mM Co(II) (Yp + Zp). This suggests that the mutation of the only methionine of CnrX led to an inability of the CnrYXH protein complex to release sufficient CnrH for *cnr* expression in the presence of nickel as the inducer.

Structural analysis of the metal binding site in Ni-bound M123A-CnrXs

X-ray structure of the metal bound soluble domain of the M123A CnrX mutant (M123A-CnrXs) was determined to demonstrate that the mutation of the methionine residue did not alter the overall fold of the protein, and particularly the structure of the metal-binding site. Although both Co-bound and Ni-bound M123A-CnrXs crystals were obtained, only the latter were of sufficient quality to collect diffraction data. The peptidic architecture of each protomer of Ni-bound M123A-CnrXs fits the all-α-fold previously determined for all forms of CnrXs.[14,40] One Ni ion was found in site 1 of each protomer (Fig. 3A). Based on

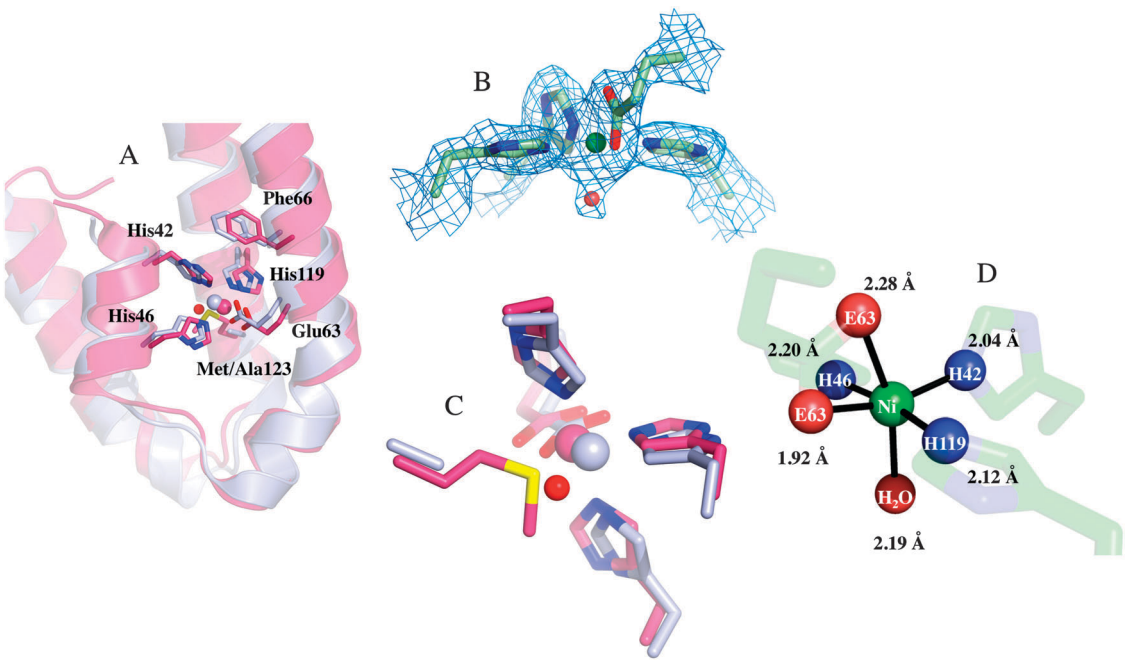

Fig. 3 Comparison of Ni-bound CnrXs with Ni-bound M123A-CnrXs, and close-up views of the Ni-binding site in the mutant protein. (A) Superimposition of the six-coordinate Ni-binding residues in CnrXs (Ni ion, backbone and side-chain in pink) and M123A-CnrXs (Ni ion, backbone and side-chains in pale blue; water molecule as a red sphere). This view includes Phe66 interacting with His119.[14] (B) $2F_0 - F_c$ electron density map contoured at 1σ of the Ni-binding ligands in M123A-CnrXs. The Ni ion and the water molecule are depicted as a green and a red sphere, respectively. (C) Close-up view showing that the thioether sulfur of Met123 and the water molecule occupy a similar position in the structures of the Ni-bound form of CnrXs and M123A-CnrXs (color code as in A). (D) Schematic representation of the Ni-binding site including the Ni–ligand distance in Å in M123A-CnrXs.

B-factor values and residuals in $F_o - F_c$ electron density maps, metal occupancy was estimated to be 55%, 100%, 60%, and 75% for chains A, B, C, and D, respectively. This poor occupancy is consistent with the loss of affinity estimated during the titration experiments (see below). A close-up view (Fig. 3B and C) of the metal-binding site of Ni-bound M123A-CnrXs in chain B shows that the Ni ion remains six-coordinate in M123A-CnrXs, with a coordination sphere composed of the ligands previously identified in the wild-type protein (His42, His46, His119 and Glu63) with the exception of the sixth coordination that is now provided by a water molecule instead of the Met123 thioether sulfur. The metal–ligand distances between the Nε2 of the three His and Ni are remarkably similar in M123A-CnrXs (Fig. 3D) and CnrXs (Table SI2, ESI†). However, the square plane is slightly distorted in the mutant protein because the equatorial O ligand from Glu63 is found at 1.92 Å instead of 2.20 Å, for CnrXs (Table SI2, ESI†). The other difference concerns the water molecule found at 2.19 Å instead of the thioether sulfur at 2.45 Å.

Ni-bound M123A-CnrXs was superimposed onto the various CnrXs conformations previously determined.[14] A close-up view of the metal binding sites (alpha carbons of His42, His46, Glu63 and His119 superimposed) shows that the metal ions are aligned along an axis (Fig. SI2, ESI†). Using the Ni bound to wild-type CnrXs as the origin of this axis on which all metal ions appeared to be aligned, Co, Ni bound to M123A-CnrXs, and Zn were located 0.1 Å, 0.2 Å and 1.5 Å away from the origin. Besides, the rmsd's for the 106 superimposed atom pairs clearly indicated that Ni-bound M123A-CnrXs dimer conformation is closest to the *apo* forms of CnrXs (rmsd < 0.5 Å) (Fig. SI2, ESI†). Consistently, crystals of Ni-bound M123A-CnrXs, of E63Q-CnrXs (PDB entry: 2y3h), and of Se-CnrXs (PDB entry: 2y3g) share the same space group ($P2_1$) and the same crystal packing (four molecules per asymmetric unit). Altogether, these observations show that Ni-bound M123A-CnrXs is different from metal-bound wild-type CnrXs while it compares very well with wild-type *apo*-CnrXs.

Spectrophotometric effects of the Met123 mutation

The H32A-CnrXs mutant previously characterized[14,15] and containing only the physiologic metal-binding site (site 1) was taken as a model of the wild-type protein. The other mutations (M123A and M123C) were introduced in this H32A background to produce the double mutants used to address the contribution of the only CnrXs methionine to the spectroscopic data.

We previously showed that the visible spectrum of Co-bound H32A-CnrXs was unusually blue-shifted and we suspected the methionine present in the coordination sphere of Co to be responsible for this shift.[15] Fig. 4 shows the comparison of H32A-, H32A-M123A-, and H32A-M123C-CnrXs loaded with two Co-equiv. or two Ni-equiv. in panel A or B, respectively. Regarding Co-bound H32A-CnrXs the spectrum displays the previously described complex ligand field envelope with an absorbance maximum centered at 495 nm and two marked shoulders at 435 and 530 nm. In the absence of the thioether sulfur (the two double-mutants), the ligand field envelope is simpler.

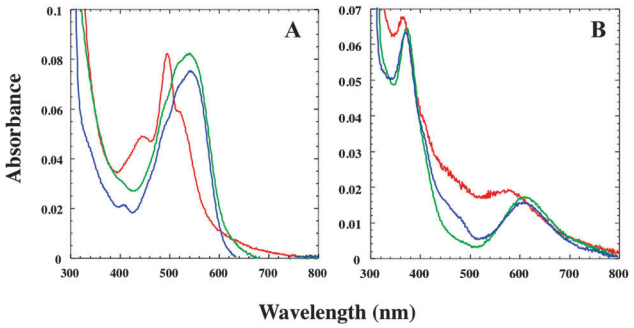

Fig. 4 UV-visible spectra of 0.5 mM H32A-CnrXs (red), H32A-M123A-CnrXs (blue) or H32A-M123C-CnrXs (green) loaded with two equiv. of $CoCl_2$ (panel A) or of $NiCl_2$ (panel B).

The spectra of the two double mutants are remarkably similar with a maximal absorbance red-shifted to 540 nm and belonging to a large featureless band (450–620 nm). The estimated molar extinction coefficient, about 70–75 M^{-1} cm^{-1}, is similar to that calculated for the single H32A-mutant. This strongly suggests that the coordination sphere is similar in the two double mutants and that Cys is not a ligand of the Co ions. Accordingly the spectrum of Co-bound H32A-M123C-CnrXs does not feature any thiolate to Co(II) ligand-to-metal charge transfer (LMCT) transition expected around 310 nm (Fig. SI3, ESI†) for a N_3O_2S(thiolate).[41] Incubation of reduced H32A-M123C-CnrXs with iodoacetamide did not result in alkylation of the cysteine residue (not shown), thus indicating that the thiol group is not accessible to the bulky carbamidomethyl moiety. This is consistent with the location of the methionine residue found buried in the protein at the bottom of the metal-binding site.[14]

When comparing the spectra of H32A- or H32A-M123A/C-CnrXs, each loaded with two Ni(II), a bathochromic shift was also observed in the absence of Met123 (Fig. 4B). The spectrum of Ni-bound H32A-CnrXs with an intense sharp band at 360 nm and a less intense and larger one around 580 nm looks reminiscent of that of Ni(II) in octahedral complex with three copies of bidentate ligand 1,2-diaminoethane ($[Ni(en)_3]^{2+}$).[42] In such an octahedral complex, the Ni(II) ion has a relatively simple magnetic behavior. Energy level diagrams and d-orbital splitting are in agreement with two unpaired electrons.[42] This was confirmed by DFT calculations, which revealed a high-spin $S = 1$ Ni(II) ion when bound in H32A-CnrXs. The triplet electronic state of Ni is thus consistent with a six-coordinate metal ion in H32A-CnrXs and likely also the double mutants, which have the same features, although red-shifted (Fig. 4B). This is consistent with the thioether sulfur ligand being replaced by a water molecule as the sixth ligand, as shown by the structure of Ni-bound M123A-CnrXs.

Both Co- and Zn-binding affinities were determined for the three proteins by chelator competition assays. Titrations were performed spectrophotometrically with fura-2 or mag-fura-2 for H32A-CnrXs and for the double mutant. Data were fit to a single binding-site model. As an example, the spectra and the corresponding fits are shown in Fig. SI4 (ESI†) for the determination

Table 1 Dissociation constants for Co and Zn determined by competition with the chromogenic chelators fura-2* and mag-fura-2**

CnrXs	Co (M)	Zn (M)
H32A	$6.54 \pm 0.74 \times 10^{-11}$*	$1.90 \pm 0.80 \times 10^{-10}$**
H32A-M123A	$1.11 \pm 0.08 \times 10^{-7}$**	$1.27 \pm 0.12 \times 10^{-9}$**
H32A-M123C	$1.60 \pm 0.19 \times 10^{-7}$**	$2.74 \pm 1.03 \times 10^{-10}$**

of the affinity of H32A- and H32A-M123A-CnrXs for Co and complete results are displayed in Table 1. H32A-CnrXs binds Co with a K_d of about 6.5×10^{-11} M while this K_d is four orders of magnitude higher when Met123 is changed for Ala or Cys. On the other hand, as expected from the fact that Met123 is not a ligand of Zn,[14] the affinity for this metal ion is poorly affected by the mutation of Met123. These results point out the crucial role of Met123 in the affinity for Co, and probably for Ni, and thus in the selectivity for the cognate metal ions.

Characterization of Co-bound M123A-CnrXs by XAS

In the absence of structural data for Co-bound M123A-CnrXs, the two Co-bound forms of H32A- and H32A-M123A-CnrXs were compared by XAS. The XANES (X-ray absorption near edge spectroscopy) spectra were compared with those of reference compounds with Co in tetrahedral and octahedral coordination as negative and positive controls, respectively. The pre-edge feature at about 7710 eV is assigned to a mixture of quadrupole 1s–3d and dipole 1s–4p transitions.[15] Its intensity is higher for 4- and 5- than for 6-coordinated complexes,[43] as shown in Fig. 5A for Co(II) acetate tetrahydrate (Co bound to six O) and Co(II)(2-methylimidazole)$_4$(BF$_4$)$_2$ (Co bound to four N). Co is six-fold coordinated in Co-bound H32A-CnrXs.[15] The pre-edge features for both Co-bound H32A-CnrXs and Co-bound H32A-M123-CnrXs are very similar, which suggests a six-fold coordination for the double mutant as well. The EXAFS (extended X-ray absorption fine structure spectroscopy) spectra and calculated fits are shown in Fig. 5B and C and the derived structural parameters are detailed in Table 2. Co-bound H32A-CnrXs was fitted with three N (His), two O (Glu) and one S (Met) ligands,[15] and structural parameters were in good agreement with the structure of site 1 determined by X-ray diffraction.

Table 2 EXAFS fit results for the two Co-bound form of H32A-CnrXs and of H32A-M123A-CnrXs

2 Co-bound CnrXs	Atom	N	R (Å)	σ^2 (Å)	R factor
H32A	His[a]	3.0	2.11	0.0040	0.016
	O	2.0	2.13	0.0090	
	S	1.0	2.57	0.0054	
H32A-M123A	His[a]	3.0	2.11	0.0050	0.038
	O	2.0	2.16	0.0050	
	S	1.0	2.63	0.0090	
	His[a]	3.0	2.10	0.0056	0.031
	O	2.0	2.15	0.0030	
	His[a]	3.0	2.07	0.0098	0.029
	O	3.0	2.13	0.0034	
	His[a]	4.0	2.10	0.0097	0.028
	O	2.0	2.13	0.0023	

N: number of atoms, R: interatomic distances, σ^2: Debye–Waller factor, R factor: residual between fit and experiment. [a] Including multiple scattering within the imidazole ring.

As expected for the mutant lacking the methionine, the peak at $R + \Delta R = 2.2$ Å corresponding to the sulfur contribution differs by a lower amplitude. The remaining contribution is due to an artifact of the Fourier transformation (side lobe) of the first peak. Indeed, a fit with the same type of environment as in Co-bound H32A-CnrXs, *i.e.* three N, two O and one S, was revealed to be unsatisfactory (R factor = 3.8×10^{-2}, Table 2). In particular, the peak at $R + \Delta R = 2.2$ Å was not correctly reproduced. Conversely, three fits of equivalent quality were obtained for H32A-M123A-CnrXs, with either five first-shell ligands (three imidazole N and two oxygen atoms) or six ligands (3N + 3O or 4N + 2O), all at a distance between 2.07 Å and 2.15 Å (Table 2). A multiple scattering contribution due to the three imidazole rings was visible at $R + \Delta R = 3$ to 4 Å, as observed for H32A-CnrXs. These structural parameters were compared to interatomic distances found for simple Co(II)-complexes from the Cambridge Structural Database

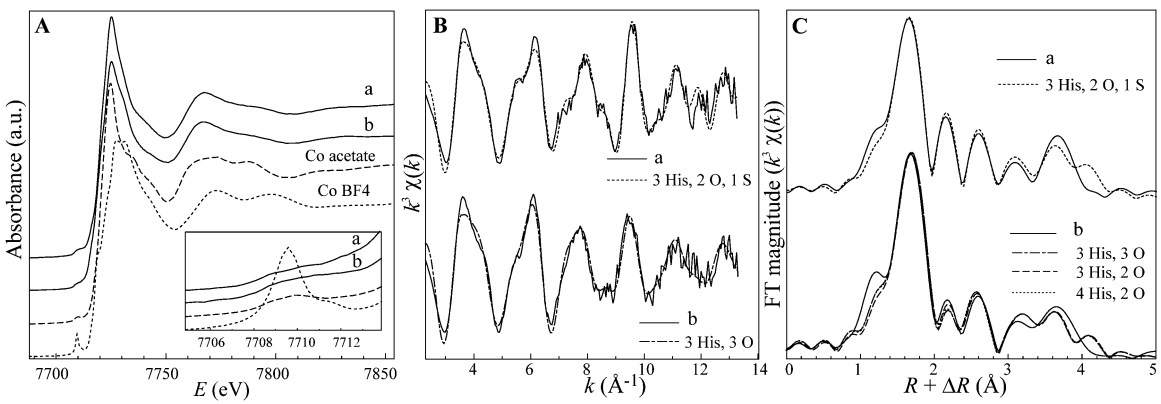

Fig. 5 Comparison of the Co K-edge XANES (A), EXAFS (B) and Fourier transformed (C) spectra of Co-bound H32A-CnrXs (a) and Co-bound H32A-M123A-CnrXs (b) loaded with two Co-equiv. A: the XANES spectra are compared with those of Co(II) acetate tetrahydrate (Co acetate) and Co(II)(2-methylimidazole)$_4$(BF$_4$)$_2$ (Co BF4). Inset: close-up view of the pre-edge feature. B, C: for 2 Co-bound H32A-CnrXs (a), the dotted line is the fit with 3 His, 2 O and 1 S ligand. For 2 Co-bound H32A-M123A-CnrXs (b), three fits of equivalent quality are shown in the FT panel (C): 3His + 3O, 3His + 2O, and 4His + 2O. For clarity, only one fit (3His + 3O) is shown in the EXAFS panel (B). The corresponding structural parameters are given in Table 1.

(CSD) (http://www.ccdc.cam.ac.uk/products/csd/). ConQuest software[44] was used to search for typical Co–O and Co–N distances in Co(II) complexes in four-, five- and six-fold coordination in CSD. The six-fold coordination was the most frequent, with 598 structures against 84 for the five-fold coordination and 161 structures for the four-fold coordination. The Co–O and Co–N distances determined in this study were consistent with those found for the six-fold coordination structures (Fig. SI5, ESI†). Thus, both the XANES and EXAFS analyses strongly suggest that Co(II) is six-coordinate when bound to H32A-M123A-CnrX.

Structure-based theoretical calculations

Two molecular models have been presented in the Experimental procedures first to study the original ligand field envelope of Co-bound H32A-CnrX and second to understand the bathochromic shifts associated with the M123A mutation: they were named Co-Met and Co-Wat, respectively. In both cases, we computed spectroscopic data for the first 30 transitions and used all of them to simulate the spectra (Tables SI3 and SI4, ESI†). Fig. 6 displays the orbital energy diagrams for both Co models. Almost all the electronic transitions occur within the beta (minority) spin set. The gap of about 1 eV between Co (lowest t_2 orbitals) and ligand orbitals below results in reduced metal(t_2)–ligand orbital mixing occurring in both Co models. Consistently, the low sensitivity of the computed transitions (positions and intensities) on fine structural features allows a good agreement between experiment and theory, as judged from the simulated *versus* experimental spectra displayed in Fig. 7. To simplify the discussion, only LMCT transitions and LFT (ligand field, *i.e.* metal–metal, transitions: $t_2 \rightarrow e$) that correspond to visible peaks in the experimental spectra are presented in Table 3.

The Co-Met simulated spectrum (Fig. 7A) nicely reproduces the main features of the experimental data, although the computed transition energies are slightly red-shifted (10 to 20 nm) in line with previous studies performed with the same ADF code and same SAOP potential.[45–47] All LMCT transitions listed below involve the Co orbital 99 (t_2 set: Fig. 6). The composition of the experimental shoulder at ~530 nm is identified with the TD-DFT transition at 554 nm. In particular, the LMCT (Met → Co) transition contributes to about 30% of the shoulder observed at 530 nm, making this shoulder the signature of the

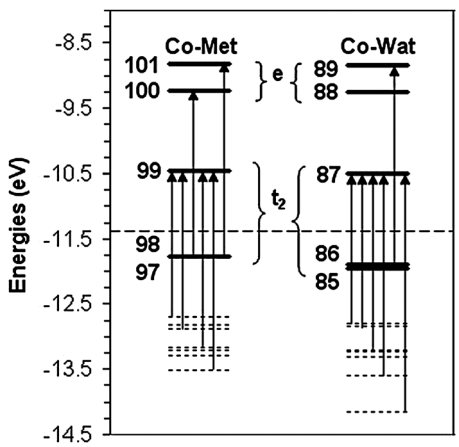

Fig. 6 Energy diagram for the orbitals of Co-Met and Co-Wat. Labels 97-101 and 85-89 refer to the (mainly) d metal orbitals of the beta (minority) spin levels for Co-Met and Co-Wat, respectively. The dashed horizontal line separates singly occupied (below) from unoccupied (above) orbitals. Co orbital energies (thick continuous lines) and the first few occupied ligand orbitals immediately below (thin dotted lines) are represented. Vertical arrows represent the main UV-visible transitions.

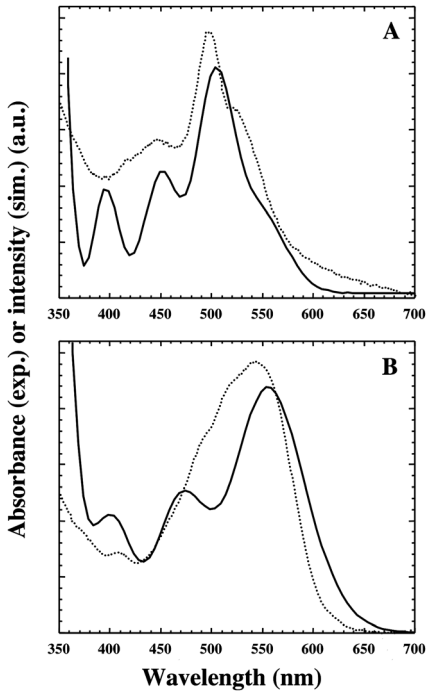

Fig. 7 Simulated spectra (solid lines) compared to experimental spectra (dotted lines). A: Co-bound H32A-CnrXs compared to Co-Met; B: Co-bound M123A-H32A-CnrXs compared to Co-Wat. For each spectrum A–B, an average broadness of the peaks has been determined visually: 1000 and 1500 cm^{-1}, respectively.

Table 3 Main spectroscopic features (transition numbers among the 30 first transitions which are computed by TD-DFT, wavelength, oscillator strength and assignment) for the two molecular models whose spectra are represented in Fig. 7

Exp	Transition #	E (nm)	Oscillator strength f (10^{-3})	Assignment
Co-Met (Co-bound H32A-CnrXs)				
~530	3[a]	554	2.216	LMCT
~495	5	508	3.756	LMCT
	6	503	3.117	LFT
~435	8	454	2.450	LMCT
Co-Wat (Co-bound M123A-H32A-CnrXs)				
~540	3[a]	560	3.981	LMCT
	4	555	1.933	LMCT
~490 (sh)	7	474	2.357	LMCT
~410	11	407	2.421	LMCT

(sh): shoulder; LMCT: ligand-to-metal charge transfer; LFT: ligand field transition. [a] The first two expected LFTs (#1–2) occur beyond 700 nm with very small predicted intensities and are not listed here. Accordingly, no visible signal appears (data not shown) in the 700–900 nm region of the experimental spectra.

methionine ligand. The experimental peak at 495 nm corresponds to a mixture of both TD-DFT transitions #5 (LMCT: 508 nm) and #6 (LFT: 503 nm). The shoulder measured at ~435 nm matches transition #8 (LMCT). The simulated spectrum (Co-Wat) is displayed in Fig. 7B (computed data summarized in Table 3) and reproduces well the experimental features. All LMCT transitions listed below involve the Co orbital 87 (t_2 set: Fig. 6). The main experimental peak around 540 nm is identified as a mixture of transitions #3 and #4 (both LMCT). The next significant peak (transition #7: LMCT) is computed at 474 nm (blue-shifted), a region where the experimental broad peak presents a shoulder (~490 nm). The last relevant feature is the simulated transition #11 (407 nm; LMCT) matching an experimental shoulder at ~410 nm.

Discussion

Bacteria must regulate gene expression in response to extracellular changes to adapt and survive to changing environmental conditions. Next to one- and two-component systems, a third means, recently acknowledged, to control the response to extracellular changes is the use of ECF-type sigma factors.[8] Very little is known about sensing extracellular metals. The CnrYXH regulation system is a prototypical example in which binding of Ni(II), and to a lesser extent of Co(II), to the sensor protein CnrX (input function) leads to the cytoplasmic release (output function) of CnrH, an ECF-sigma factor sequestered at the membrane so far. This process is mediated by the transmembrane anti-sigma factor CnrY. In contrast, the question of how the concentration of metal ions is sensed and regulated in the cytoplasm has been extensively reviewed. The DNA-binding metal-responsive transcriptional regulators involved in these processes combine two functions in a single polypeptide chain. The input function (sensing) is to bind the cognate metal ion and to transmit the output function (co-repression, de-repression or activation) by modulating the interaction of the regulator with dedicated DNA sequences placed upstream of the regulated genes. This interaction is allosterically regulated by the conformational changes that are driven by the specific binding of the cognate metal, the nature and the structure of the first coordination shell around the cognate metal being the major determinant of the biological specificity.[41,48–53] We have reported in a previous work the coordination sphere of the metal ions sensed by CnrXs and the resulting allosteric changes in the protein.[14] The main conclusion was that the mechanism deduced from these results is in agreement with the concept of metal selectivity and allosteric switching developed for the metalloregulatory proteins with the ligand selection leading to differential coordination number/geometry and playing a crucial role in discriminating cognate (Ni or Co in CnrX) from non-cognate metals (here, Zn). However the metal-binding site in CnrX includes the only methionine (M123) of the protein. To the best of our knowledge the use of the thioether sulfur of a methionine residue in the coordination sphere of a bacterial sensor known to regulate the traffic of Ni and/or Co is unprecedented.

In this report, the role of Met123 as a trigger of the signal transduction was pointed out by *in vivo* studies. The Yp + Zp experiment where expression of CnrYXH was enforced by an RpoD-dependent RNA-polymerase served as a control of stability of the expressed proteins. In that case, expression of the proteins and their regulation are uncoupled. With wild-type CnrX, the increase in both metal resistance and β-galactosidase activity in the presence of Ni as an inducer showed that CnrH was stable enough to get to the *cnrCp* promoter. With the CnrX derivative, the CnrYXH protein complex was unable to release sufficient CnrH for *cnr* expression although the presence of M123A-CnrX was confirmed by Western blot. This ruled out the hypothesis that M123A-CnrX could be degraded post-translationally, thus demonstrating that this protein was ineffective in signal transduction. These controls allow the following reading: in the Yp − Zp experiment, where transcription initiation depends only on CnrH, CnrH sits immobilized on CnrXY and does not enter the positive cooperative loop of regulation when CnrX is altered by the M123A mutation. This conclusion is consistent with the fact that M123A-CnrX should have retained the ability to bind metal ions *in vivo*, although with a lower affinity compared to the wild-type protein, as M123A-CnrXs did *in vitro*. Moreover, the all-α-fold previously determined for all forms of CnrXs[14,40] is maintained in Ni-bound M123A-CnrXs whose conformation is close to that of *apo*-CnrXs. Yet upon superimposition of the metal binding sites, it appears that both Ni binding sites are highly similar (both Ni ions laid 0.2 Å apart) with the Ni ion bound to M123A-CnrXs located in-between Zn (1.3 Å away) and Ni/Co (0.2 Å away) bound to wild-type CnrXs. Ni is unable to activate M123A-CnrXs like Zn is unable to activate wild-type CnrXs because it does not count Met123 as a ligand.[14] In contrast, the agonists of wild-type CnrXs, Ni and Co, recruit the methionine in their coordination sphere. This suggests that the M123A mutant protein is defective in metal-dependent allosteric switching. Moreover, combining a close-to-active metal binding site to a close-to-inactive conformation, the structure of Ni-bound M123A-CnrXs supports the role of the Met side chain as a trigger of the conformational change priming signal transduction. As a consequence, the M123A derivative of CnrX is no longer able to propagate the signal *in vivo* and CnrH does not reach the RNA-polymerase.

In the absence of an X-ray structure for Co-bound M123A-CnrXs, XAS data gave relevant indications. It should be noticed that the Ni–His distances deduced from the X-ray data are in the range of the average of the Co–His distances estimated by fitting the EXAFS data (Table 2, fit 3N3O). This strongly suggests that the Ni-binding site and the Co-binding site in M123A-CnrXs are almost identical, as observed for the wild-type protein.[14] Moreover, in the absence of a model structure for the simulation of the electronic absorption spectrum of Co-bound M123A-CnrXs, satisfactory results were obtained using the same metal–O_{Wat} distance as for Ni-bound M123A-CnrXs (*i.e.* 2.2 Å). This suggests that in the absence of methionine, the metal–O_{Wat} distance is in the same range for both metal ions, as was the metal–thioether sulfur distance in the presence of methionine.[14]

The thioether sulfur of the methionine as an original ligand also has a direct consequence on the electronic absorption spectra that display a hypsochromic shift upon binding of either Co or

Ni compared to the already known systems involving only N–O ligands. A good reproduction of the experimental spectra through molecular model-based TD-DFT calculations was obtained. As the structure-based models involve only the direct ligands of Co, the structural information contained in the UV-visible spectra concerns essentially the first shell of coordination. One essential consequence is that relevant structural information could be obtained from simulation of spectra deduced from theoretical models. Except for its influence on the value of the wavelength corresponding to the absorbance maximum, the contribution of the methionine is quite discreet but still detectable. For instance, the LMCT (Met → Co) transition contributes to 30% of the shoulder observed at 530 nm for Co-bound H32A-CnrXs.

The decrease in affinity, estimated for Co(II), linked to substitution of Met123 for Ala or Cys shows that Met123 is a major determinant of the affinity, besides of the selectivity, of the cognate metals for CnrX. In addition, both the UV-visible characterization of Co-bound H32A-M123C-CnrXs and the estimation of the affinity of this metal ion for this double mutant strongly suggest that the Cys residue, with a shorter side chain, is not a ligand. The coordination sphere of the metal sensor CnrX can be compared to that of the nickel- and cobalt-responsive metalloregulator RcnR, or of the Ni(II)-responsive transcriptional repressor NikR, both from *E. coli*, that use a strategic cysteine residue. RcnR forms six-coordinate complexes with its cognate metal ions, Ni(II) and Co(II), to regulate the expression of the exporter RcnA and the periplasmic protein RcnB *in vivo* in *E. coli*.[54–56] The coordination sphere was characterized as $(N/O)_5S$ with S corresponding to the thiolate of the only cysteine residue in the protein. The NikR tetramer contains one high-affinity site for Ni per monomer.[53] Ni(II) forms the N_3S_1 four-coordinate square planar complexes required to activate the DNA binding function of NikR *in vivo*.[57] Interestingly, the response of these metalloregulators seems to be partly dependent on the S–metal distance. In NikR, the S–metal distance is proposed to be involved in the discrimination between the cognate Ni(II) (S–Ni = 2.13 Å) and the non-cognate Cu(II) (S–Cu = 2.21 Å), both being in a four-coordinate planar geometry.[58] In RcnR, the differential recognition of the two cognate metals involves the S–metal distance (2.31 Å for Co(II) and 2.62 Å for Ni(II)) along with the number of His imidazole ligands, even if both Ni and Co are six-coordinate.[54] In CnrX, the S–Metal distance was also previously suggested to be crucial to fine-tune the discrimination between the different active forms. Actually Ni, Co and Cu elicit a biological response in inverse proportion to this distance (the shortest the distance, the strongest the response: Ni–S = 2.45 Å;[14] Co–S = 2.54 Å;[14] Cu–S = 2.77 Å[37]). With a S–metal distance of 3.9 Å, Met123 is not a ligand of the non-cognate ion Zn(II) that forms an unresponsive complex with CnrX.[14] Indeed, Zn was consistently identified as a poor inducer by either transcriptomic[2,11] or proteomic studies.[14] The two-order of magnitude decrease in affinity, estimated for Co(II), linked to substitution of Met123 for Ala shows that Met123 is a major determinant of the affinity, besides of the selectivity, of the cognate metals for CnrX.

In conclusion, M123 is required for allosteric switching, thus in line with the connection of coordination chemistry with biological function, and nature's use of a Met rather than a Cys is likely important for redox stability in the periplasm. This is consistent with the strict conservation of a methionine in the alignment of the 23 identified members of the CnrX family.[14]

Acknowledgements

We are grateful to the staff at the BM30B (FAME) and ID23-2 beamlines at the European Synchrotron Radiation Facility (ESRF, Grenoble, France) for their help during the XAS experiments and the X-ray data collection, respectively. We also thank Jean-Marc Latour and Isabelle Michaud-Soret from the LCBM (UMR 5249, Grenoble) and David Tierney from the University of New Mexico for sharing several Co reference compounds and spectra. We thank Grit Schleuder for skillful technical assistance during *in vivo* studies, and Crystal Lee Young for her help in copy editing the manuscript.

References

1 M. Mergeay, D. Nies, H. G. Schlegel, J. Gerits, P. Charles and F. Van Gijsegem, *J. Bacteriol.*, 1985, **162**, 328–334.
2 S. Monchy, M. A. Benotmane, P. Janssen, T. Vallaeys, S. Taghavi, D. van der Lelie and M. Mergeay, *J. Bacteriol.*, 2007, **189**, 7417–7425.
3 T. von Rozycki and D. H. Nies, *Antonie van Leeuwenhoek*, 2009, **96**, 115–139.
4 P. J. Janssen, R. Van Houdt, H. Moors, P. Monsieurs, N. Morin, A. Michaux, M. A. Benotmane, N. Leys, T. Vallaeys, A. Lapidus, S. Monchy, C. Médigue, S. Taghavi, S. McCorkle, J. Dunn, D. van der Lelie and M. Mergeay, *PLoS One*, 2010, **5**, e10433.
5 D. H. Nies, *FEMS Microbiol. Rev.*, 2003, **27**, 313–339.
6 T. von Rozycki, D. H. Nies and M. H. Saier Jr, *Comp. Funct. Genomics*, 2005, **6**, 17–56.
7 T. Masher, J. D. Helmann and G. Unden, *Microbiol. Mol. Biol. Rev.*, 2006, **70**, 910–938.
8 A. Staroń, H. J. Sofia, S. Dietrich, L. E. Ulrich, H. Liesegang and T. Mascher, *Mol. Microbiol.*, 2009, **74**, 557–581.
9 C. Grosse, S. Friedrich and D. H. Nies, *J. Mol. Microbiol. Biotechnol.*, 2007, **12**, 227–240.
10 H. Liesegang, K. Lemke, R. A. Siddiqui and H. G. Schlegel, *J. Bacteriol.*, 1993, **175**, 767–778.
11 G. Grass, C. Grosse and D. H. Nies, *J. Bacteriol.*, 2000, **182**, 1390–1398.
12 C. Tibazarwa, S. Wuertz, M. Mergeay, L. Wyns and D. van Der Lelie, *J. Bacteriol.*, 2000, **182**, 1399–1409.
13 G. Grass, B. Fricke and D. H. Nies, *Biometals*, 2005, **18**, 437–448.
14 J. Trepreau, E. Girard, A. P. Maillard, E. de Rosny, I. Petit-Haertlein, R. Kahn and J. Covès, *J. Mol. Biol.*, 2011, **408**, 408–766.
15 J. Trepreau, E. de Rosny, C. Duboc, G. Sarret, I. Petit-Harlein, A. P. Maillard, A. Imberty, O. Proux and J. Covès, *Biochemistry*, 2011, **50**, 9036–9045.
16 J. Salgado, H. R. Jiménez, A. Donaire and J. M. Moratal, *Eur. J. Biochem.*, 1995, **231**, 358–369.

17 A. Donaire, B. Jiménez, J. Moratal, J. F. Hall and S. S. Hasnain, *Biochemistry*, 2001, **40**, 837–846.
18 M. E. Kovach, P. H. Elzer, D. S. Hill, G. T. Robertson, M. A. Faris, R. M. Roop 2nd and K. M. Peterson, *Gene*, 1995, **166**, 175–176.
19 D. H. Nies, A. Nies, L. Chu and S. Silver, *Proc. Natl. Acad. Sci. U. S. A.*, 1989, **86**, 7351–7355.
20 D. H. Nies, M. Mergeay, B. Friedrich and H. G. Schlegel, *J. Bacteriol.*, 1987, **169**, 4865–4868.
21 J. Sambrook, E. F. Fritsch and T. Maniatis, *Molecular cloning, a laboratory manual*, Cold Spring Harbor Laboratory, Cold Spring Harbor, NY, 1989.
22 R. Simon, U. B. Priefer and A. Pühler, *Nat. Biotechnol.*, 1983, **1**, 784–791.
23 D. H. Nies, *J. Bacteriol.*, 1992, **174**, 8102–8110.
24 M. M. Bradford, *Anal. Biochem.*, 1976, **72**, 248–254.
25 P. Kuzmic, *Methods Enzymol.*, 2009, **467**, 247–280.
26 M. V. Golynskiy, W. A. Gunderson, M. P. Hendrich and S. M. Cohen, *Biochemistry*, 2006, **45**, 15359–15372.
27 Z. Xiao and A. G. Wedd, *Nat. Prod. Rep.*, 2010, **5**, 768–789.
28 W. Kabsch, *Acta Crystallogr.*, 2010, **D66**, 125–132.
29 Collaborative Computational Project Number 4, *Acta Crystallogr., Sect. D: Biol. Crystallogr.*, 1994, **50**, 760–763.
30 P. A. Karplus and K. Diederichs, *Science*, 2012, **336**, 1030–1033.
31 T. C. Terwilliger, R. W. Grosse-Kunstleve, P. V. Afonine, N. W. Moriarty, P. H. Zwart, L.-W. Hung, R. J. Read and P. D. Adams, *Acta Crystallogr.*, 2008, **D64**, 61–69.
32 A. J. McCoy, R. W. Grosse-Kunstleve, P. D. Adams, M. D. Winn, L. C. Storoni and R. J. Read, *J. Appl. Crystallogr.*, 2007, **40**, 658–674.
33 K. D. Cowtan and P. Main, *Acta Crystallogr.*, 1996, **D52**, 760–763.
34 K. D. Cowtan, *Acta Crystallogr.*, 2006, **D62**, 1002–1011.
35 P. Emsley and K. Cowtan, *Acta Crystallogr.*, 2004, **D60**, 2126–2132.
36 G. Te Velde and E. J. Baerends, *J. Comput. Phys.*, 1992, **99**, 84–98.
37 O. V. Gritsenko, P. R. T. Schipper and E. J. Baerends, *Chem. Phys. Lett.*, 1999, **302**, 199–207.
38 F. Kootstra, P. L. de Boeij and J. G. Snijders, *J. Chem. Phys.*, 2000, **112**, 6517–6531.
39 P. Romaniello and P. L. de Boeij, *Phys. Rev.*, 2005, **B71**, 155108.
40 G. Pompidor, A. P. Maillard, E. Girard, S. Gambarelli, R. Kahn and J. Covès, *FEBS Lett.*, 2008, **582**, 3954–3958.
41 J. S. Iwig, S. Leitch, R. W. Herbst, M. J. Maroney and P. T. Chivers, *J. Am. Chem. Soc.*, 2008, **130**, 7592–7606.
42 A. F. Cotton and G. Wilkinson, *Advanced inorganic chemistry, a comprehensive text*, Wiley-Interscience Publication, New York, 5th edn, 1988.
43 A. Adrait, L. Jacquamet, L. Le Pape, A. Gonzalez de Peredo, D. Aberdam, J.-L. Hazemann, J.-M. Latour and I. Michaud-Soret, *Biochemistry*, 1999, **39**, 6248–6260.
44 I. Bruno, J. Cole, P. Edgington, M. Kessler, C. Macrae, P. McCabe, J. Pearson and R. Taylor, *Acta Crystallogr.*, 2002, **B58**, 389–397.
45 A. Rosa, G. Ricciardi, E. J. Baerends and S. J. A. van Gisbergen, *J. Phys. Chem. A*, 2001, **105**, 3311–3327.
46 E. J. Baerends, G. Ricciardi, A. Rosa and S. J. A. van Gisbergen, *Coord. Chem. Rev.*, 2002, **230**, 5–27.
47 I. Infante and F. Lelj, *Chem. Phys. Lett.*, 2003, **367**, 308–318.
48 D. P. Giedroc and A. I. Arunkumar, *Dalton Trans.*, 2007, 3107–3120.
49 Z. Ma, F. E. Jacobsen and D. P. Giedroc, *Chem. Rev.*, 2009, **109**, 4644–4681.
50 K. J. Waldron and N. J. Robinson, *Nat. Rev. Microbiol.*, 2009, **7**, 25–35.
51 H. Reyes-Caballero, G. C. Campanello and D. P. Giedroc, *Biophys. Chem.*, 2011, **156**, 103–114.
52 A. J. Guerra and D. P. Giedroc, *Arch. Biochem. Biophys.*, 2012, **519**, 210–222.
53 M. A. Pennella, A. I. Arunkunar and D. P. Giedroc, *J. Mol. Biol.*, 2006, **356**, 1124–1136.
54 A. Rodrigue, G. Effantin and M.-A. Mandrand-Berthelot, *J. Bacteriol.*, 2005, **187**, 2912–2916.
55 K. A. Higgins, P. T. Chivers and M. J. Maroney, *J. Am. Chem. Soc.*, 2012, **134**, 7081–7093.
56 J. S. Iwig and P. T. Chivers, *Nat. Prod. Rep.*, 2010, **27**, 658–667.
57 E. R. Schreiter, M. D. Sintchak, Y. Guo, P. T. Chivers, R. T. Sauer and C. L. Drennan, *Nat. Struct. Biol.*, 2003, **10**, 794–799.
58 S. Leitch, M. J. Bradley, J. L. Rowe, P. T. Chivers and M. J. Maroney, *J. Am. Chem. Soc.*, 2007, **129**, 5085–5095.